View metadata, citation and similar papers at core.ac.uk

brought to you by CORE

provided by Elsevier - Publisher Connector

Structure, Vol. 10, 1051–1062, August, 2002, ©2002 Elsevier Science Ltd. All rights reserved. PII S0969-2126(02)00797-9

Crystal Structure of Recombinant Human Interleukin-22

Ronaldo Alves Pinto Nagem,[1,2] Didier Colau,[3] Laure Dumoutier,[3] Jean-Christophe Renauld,[3] Craig Ogata,[4] and Igor Polikarpov[1,5,6]

[1]Laboratório Nacional de Luz Síncrotron
Caixa Postal 6192
CEP 13084-971
Campinas, São Paulo
Brazil

[2]Universidade Estadual de Campinas
Deptartamento de Física
Caixa Postal 6165
CEP 13084-971
Campinas, São Paulo
Brazil

[3]Ludwig Institute for Cancer Research
Brussels Branch and
The Experimental Medicine Unit
Christian de Duve Institute of Cellular Pathology
Université de Louvain
Brussels
Belgium

[4]Brookhaven National Laboratory
Howard Hughes Medical Institute
NSLS
Upton, New York 11973

[5]Instituto de Física de São Carlos
Universidade de São Paulo
Avenida Trabalhador Sãocarlense 400
CEP 13560-970
São Carlos, São Paulo
Brazil

Summary

Interleukin-22 (IL-10-related T cell-derived inducible factor/IL-TIF/IL-22) is a novel cytokine belonging to the IL-10 family. Recombinant human IL-22 (hIL-22) was found to activate the signal transducers and activators of transcription factors 1 and 3 as well as acute phase reactants in several hepatoma cell lines, suggesting its involvement in the inflammatory response. The crystallographic structure of recombinant hIL-22 has been solved at 2.0 Å resolution using the SIRAS method. Contrary to IL-10, the hIL-22 dimer does not present an interpenetration of the secondary-structure elements belonging to the two distinct polypeptide chains but results from interface interactions between monomers. Structural differences between these two cytokines, revealed by the crystallographic studies, clearly indicate that, while a homodimer of IL-10 is required for signaling, hIL-22 most probably interacts with its receptor as a monomer.

Introduction

Interleukin-22 (IL-22) is a novel protein that was recently identified in murine cells [1] and was subsequently found in human cells [2]. In vitro experiments showed that IL-22 expression is induced by interleukin-9 (IL-9) in T cells and mast cells [1]. IL-9 induction is rapid (within 1 hr) and does not require protein synthesis. IL-22 was initially classified as a cytokine due to several characteristic features: the presence of an N-terminal hydrophobic signal peptide, ~20 kDa in size, and a low, but detectable, amino acid identity with interleukin-10 (IL-10). This fact was later confirmed by the finding that the IL-22 receptor complex consists of two members of the class II cytokine receptor family, namely, CRF2-9 and CRF2-4 or IL-10Rβ [3, 4]. Other members of the class II family are the two interferon-γ (IFN-γ) receptor chains (Rα and Rβ), the two chains of the IL-20 receptor (Rα and Rβ), the two chains of the IFN-α/β receptor, the interleukin-10 receptor (IL-10R1), and the tissue factor [5]. On the other hand, the growth hormone (GH) receptor and the prolactin receptor, among others, are members of the class I cytokine receptor family.

IL-22 is a member of interleukin-10 family of cytokines, which also includes IL-19 [6], IL-20 [7], and IL-24 [8] in addition to IL-10 [9] and a number of its viral homologs [10]. The members of the IL-10 family have sequence identities of 20%–27% with human cellular paralogs, whereas amino acid sequence identity between homologs from different organisms can be as high as 70%–80% [10].

Human and mouse IL-22 (hIL-22 and mIL-22) have 179 residues, including four cysteines, and share 79% amino acid sequence identity. On the other hand, the hIL-22 (mIL-22) sequence has only 25% (22%) identity with human IL-10 (hIL-10). Most of the conserved residues between IL-22 and IL-10 are located in the C-terminal half of the protein, which has been found to be critical for IL-10 activity, leading to the hypothesis that IL-22 and IL-10 may share common or related biological activities. The only three-dimensional structures of members of the IL-10 family of cytokines known at present are those of IL-10 [11, 12, 13] and its viral homolog from Epstein-Barr virus (EBV) [14].

The fact that mIL-22 is induced in various organs by lipopolysaccharide (LPS) suggests that the role of this new cytokine is not restricted to the immune system [2]. It was also found that hIL-22 activates the signal transducers and activators of transcription factors 1 and 3 in several hepatoma cell lines. IL-22 stimulation of HepG2 human hepatoma cells upregulated the production of acute phase reactants, such as serum amyloid A, α1-antichymotrypsin, and haptoglobin [2]. A similar acute phase reactant induction was also observed in mouse liver upon IL-22 injection, suggesting involvement of IL-22 in the inflammatory response. In addition, IL-22 might play a role in allergy and asthma due to the involvement of IL-9 in these two pathologies [15, 16]. Furthermore, the IL-22 gene is located on human chromosome 12q [17], where several loci potentially linked to asthma have been identified by genetic studies [18].

[6]Correspondence: ipolikarpov@if.sc.usp.br

Key words: crystal structure; IL-22; IL-TIF; IL-10; IFN-γ; interleukin

Cytokines exert their actions by binding to specific cell surface receptors, leading to the activation of cytokine-specific signal transduction pathways. Recent results [3, 4] show that the functional IL-22 receptor complex consists of two receptor chains, the CRF2-9 (IL-22R) chain and the CRF2-4 (IL-10R2 or IL-10Rβ) chain. The latter has been demonstrated to be a functional component of the IL-10 signaling complex [19]. This is the first example within the class II cytokine receptor family of a receptor being utilized as a component of multiple distinct cytokine signaling complexes. A similar sharing is also observed in IL-2, IL-4, IL-7, IL-9, and IL-15 receptor complexes (γ common chain, γ_c).

Here we describe the structure of recombinant hIL-22 refined to 2.0 Å resolution and its comparison with the crystallographic models of hIL-10 [11, 12, 13] and hIFN-γ [20]. The possible receptor binding sites were inferred on the basis of structural comparison with the hIFN-γ/hIFN-γRα complex [20], the recently determined complex of IL-10 with its receptor IL-10R1 [21], and amino acid sequence alignments. Structural comparisons with IL-10 and IFN-γ receptor complexes clearly indicate that, while a homodimer of IL-10 and/or IFN-γ is required for signaling, hIL-22 most probably interacts with its receptor as a monomer.

Results and Discussion

Structure Determination

Purified recombinant hIL-22 was crystallized at the Protein Crystallography Laboratory of the Brazilian National Synchrotron Light Laboratory (LNLS) using the hanging drop method. Several attempts to improve crystal quality were performed, including pH and precipitant concentration refinement, detergent addition, and macroseeding. Well-diffracting crystals were obtained using sodium tartrate and TRITON X-100 detergent in HEPES buffer at pH 7.5. The crystal space group was determined to be $P2_12_12_1$ (see Experimental Procedures for details).

The structure of hIL-22 was solved by X-ray diffraction using the SIRAS method. The data sets of an iodine derivative (I-hIL-22) and a native crystal (Nat-hIL-22) were collected at the Protein Crystallography beamline [22, 23] at the LNLS (Campinas, São Paulo, Brazil). The I-hIL-22 derivative was prepared according to the quick-cryosoaking procedure [24, 25] for fast derivatization of protein crystals. One additional Hg derivative data set was collected at the X4A beamline at NSLS (Upton, New York). These data did not provide a strong isomorphous or anomalous signal and were therefore used only at the later stages of refinement and during the construction of disordered loops, as a quasi-native data set. Details of the preparation of native and derivative crystals for data collection as well as data statistics are given in Table 1.

SIRAS-derived phases using native and iodine derivative data have a mean figure of merit of 0.45 in the resolution range from 21.7 to 2.4 Å. Due to the high resolution and completeness of the I-hIL-22 data set and the quality of the solvent-flattened electron density map, automatic construction of an hIL-22 hybrid model could be performed by the ARP/wARP program [26]. The inferred amino acid sequence derived from the cDNA [2] was used in the final model side chain assignment.

Quality of the Model

The initial structure of hIL-22 was improved by a number of cycles of refinement and rebuilding using the CNS package [27]. The final model is characterized by an R factor of 0.188 and an R_{free} of 0.22 for the Nat-hIL-22 data in the resolution range from 21.7 to 2.0 Å.

The isolated cDNA of hIL-22 encodes a protein of 179 amino acids, the first 33 of which are predicted to function as a signal sequence [3]. The N-terminal amino acid analysis of hIL-22 confirms that the mature protein begins at amino acid residue 34. The refined model of hIL-22, a dimer in the asymmetric unit (Figure 1), includes monomer A, with 142 amino acid residues (Ser38–Ile179), monomer B, with 141 amino acid residues (His39–Ile179), and 189 water molecules. A total of 93.8% and 6.2% of the amino acid residues adopt a conformation corresponding to the most favored and additionally allowed regions of the Ramachandran plot, respectively (see Table 2 for further information about refinement and geometry statistics). No residues have been encountered in the disallowed regions of the Ramachandran plot. Pro113 is in the *cis* conformation. Alternative conformations of the side chains were found for residues Met172 (monomer A) and Asp43, Ser45, Arg55, Ile75, His81, Arg124, Ile161, and Leu174 (monomer B). The electron density for part of loop DE (residues 127–132) is weak, resulting in high temperature factors for this part of the protein (Figure 2).

Each monomer of the hIL-22 model, as shown in Figure 1B, is characterized by six α helices (A–F) that fold in a compact bundle. Helix A (amino acid residues Lys44–Ser64) is linked to a short helix, B (Glu77–Phe80), by a large loop, AB (Leu65–Gly76). Helix A has a kink at Gln48–Gln49, presumably due to a hydrogen bond between Nε-Gln49 and O-Ser45 (2.79 Å and 2.55 Å in monomers A and B, respectively). This divides helix A into two unequal parts: A_1 and A_2. Loop BC (His81–Glu87) connects helix B to helix C (Arg88–Glu102). Helix C is joined to helix F by a disulfide bond between Cys89 and Cys178. Another loop (CD; Val103–Tyr114) links helix C to helix D (Met115–Leu129). According to PROCHECK [28], a small difference in secondary structure between monomers is observed at the loop CD region. A small α helix is observed between amino acid residues Phe105 and Gln107 of monomer B. Helix D is connected to helix E by a disordered loop (DE; Ser130–Asp138). This loop is stabilized, at least in the vicinity of Cys132, by another disulfide bond between Cys132 and Cys40, the latter in the N-terminal coil. Finally, a simple junction EF (Gly156) joins the last two helices, E (Leu139–Leu155) and F (Glu157–Cys178). Probably, as a consequence of a disulfide bond between Cys89 and Cys178, the latter belonging to the C-terminal of helix F, a kink at Glu166 divides helix F into two parts: F_1 and F_2.

Dimer Formation

A significant part (61%) of the volume of the asymmetric unit (6.27×10^4 Å^3) is occupied by a dimer of hIL-22. A small fraction of this volume (8%) is filled with ordered

Table 1. Details of the Preparations and Data Collection Statistics of hIL-22 Crystals

	Nat-hIL-22	I-hIL-22	Hg-hIL-22 (Quasi-Native)
Wavelength (Å)	1.54	1.54	1.54
Space group	$P2_12_12_1$	$P2_12_12_1$	$P2_12_12_1$
Unit cell parameters (Å)	a = 55.43, b = 61.61, and c = 73.47	a = 56.05, b = 61.78, and c = 73.63	a = 56.04, b = 61.71, and c = 74.61
Resolution (Å)	21.7–2.00 (2.05–2.00)	21.8–1.92 (1.96–1.92)	22.4–1.90 (1.97–1.90)
Number of reflections	61,846	182,876	55,855
Number of unique reflections[a]	16,382	37,777	29,854
$<I/\sigma(I)>$	14.5 (3.8)	13.4 (3.1)	8.2 (2.1)
Multiplicity	3.8 (3.4)	4.8 (4.3)	1.9 (1.7)
Completeness	92.7 (82.3)	99.9 (99.7)	75.9 (77.9)
R_{merge}[b]	8.2 (35.0)	11.7 (43.9)	10.0 (49.9)
Data collected (degrees)	103	248	70
Cryoprotectant solution	mother liquor 15% ethylene glycol	mother liquor 15% ethylene glycol 0.125 M NaI	mother liquor 15% ethylene glycol 5 mM $HgCl_2$
Soaking time	30 s	180 s	10 hr

Statistical values for the highest resolution shells are shown in parentheses.
[a] Multiplicity of derivative (native) data sets calculated with Friedel-related reflections treated separately (as equivalent).
[b] $R_{merge} = \Sigma_{hkl}|I_{hkl} - <I_{hkl}>|/\Sigma_{hkl} I_{hkl}$.

water molecules. The monomers are essentially equal; however, a number of significant differences in the main chain conformation in the vicinity of amino acid residues Gln48, Asn69, Gly136, and Lys154 are observed (Figure 2). These differences could mostly be explained by crystallographic and noncrystallographic contacts. The reason for a significant positional difference between monomers around Gln48 is the fact that this region in monomer A is involved in interface interactions, while the same region in monomer B is exposed to the solvent. Besides this, the presence of two intramolecular interactions (Oδ1-Asp43/Oγ-Ser45 at a distance of 2.64 Å in monomer A and O-Asn46/Nε2-Gln49 at 2.55 Å in monomer B) contributes to a relative change in main chain atomic positions between residues Leu42 and Pro50. The second conformational difference, around residue Asn69, is a consequence of a crystallographic contact between side chain atoms of Asn69 and Thr70 of monomers A and B, respectively. Gly136 is localized in disordered loop DE. This fact explains the rmsd (root mean square deviation) of around 2.0 Å in the vicinity of this residue. Finally, the last major difference between monomers is found close to Lys154. In this region three distinct interactions of Lys153 and Lys154 from monomer B (Oε1-Glu102/Nζ-Lys153 at a distance of 2.68 Å, Oδ1-Asn46/Nζ-Lys153 at 2.78 Å, and Oε1-Glu160/Nζ-Lys154 at 2.80 Å), which are absent in monomer A, are responsible for a high rmsd of main chain atoms.

Unlike hIL-10, the hIL-22 dimer does not result from the intertwining of the main chain of each monomer

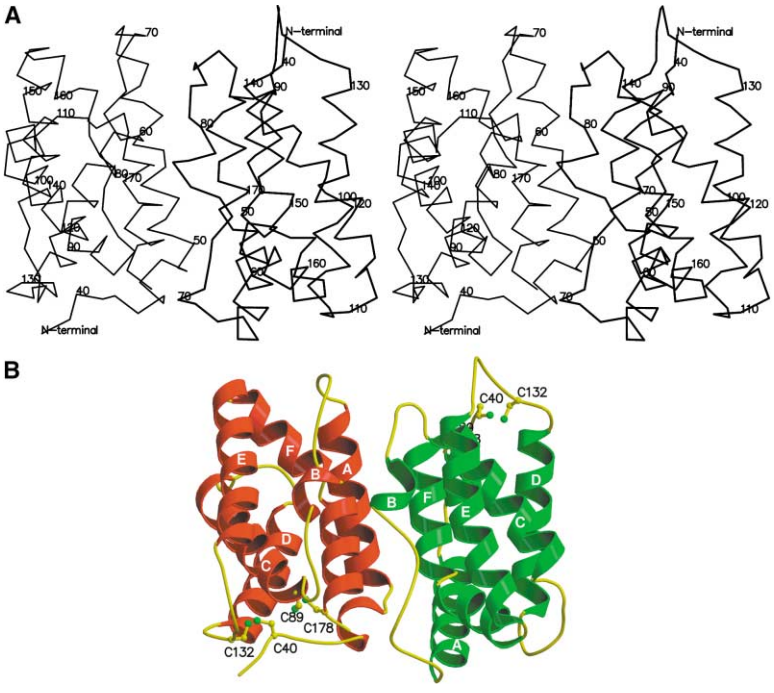

Figure 1. Structure of the IL-22 Dimer

(A) Stereo view of the C_α trace of the dimeric structure of hIL-22.

(B) Schematic representation of the secondary structure of the hIL-22 dimer, according to PROCHECK [28], showing the location of the two disulfide bonds (Cys40-Cys132 and Cys89-Cys178) represented by ball and stick diagrams. The figures were prepared using Molscript [29], Bobscript [30], and Raster3D [31].

Table 2. Refinement Statistics and Quality of the hIL-22 Model

Refinement Statistics	
Resolution range (Å)	21.7–2.0
Total number of reflections	15,684
Working set number of reflections	14,892
R factor (%)	18.8
Test set number of reflections	792
R_{free} (%)	22.0
Total number of protein atoms	2330
Total number of water molecules	189
Stereochemical Parameters	
Rmsd bond distances (Å)	0.006
Rmsd bond angles (°)	1.1
Average B factors	
Residue atoms (Å²) (A, B)	24.3 (22.3, 26.2)
Main chain atoms (Å²) (A, B)	22.1 (20.2, 24.1)
Side chain atoms (Å²) (A, B)	26.3 (24.4, 28.1)
Water molecules (Å²)	37.3
Average B factor rmsd	
Residue atoms (Å²) (A, B)	2.5 (2.6, 2.5)
Main chain atoms (Å²) (A, B)	1.0 (1.0, 1.0)
Side chain atoms (Å²) (A, B)	1.9 (2.0, 1.8)
Water molecules (Å²)	11.4
Noncrystallographic Symmetry[a]	
Rmsd coordinates	
Cα atoms (Å)	0.911
Main chain atoms (Å)	0.884
All bonded atoms (Å)	1.670
Rmsd B factors	
Cα atoms (Å²)	10.04
Main chain atoms (Å²)	10.05
All bonded atoms (Å)	10.77

[a] Between subunits A and B.

(Figure 1). An interface area of approximately 2250 Å², which corresponds to 30% of the total surface area of a monomer, is involved in the dimer formation. The buried surface for the chosen dimer conformation is at least twice that of any other possible dimer generated as a result of crystal packing (~960 Å² or less). Besides this, the dimer interface, which is formed mostly by residues Arg41–Phe80 and Asp168–Ile179 in monomer A and

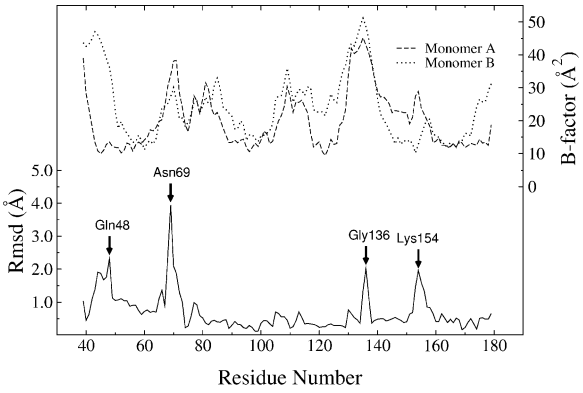

Figure 2. Least-Square Fit of Monomer A to Monomer B and Temperature Factors Plots

The root mean square deviation (rmsd) and B factors are shown as a function of residue number. Only main chain atoms were used in the calculation.

Table 3. Intermolecular Contacts

Monomer A		Monomer B		
Residue	Atom	Residue	Atom	Distance (Å)
Arg175	Nη2	Glu166	Oε1	2.57
Phe57	O	Asn176	Nδ2	2.64
Arg73	Nη2	Val83	O	2.71
Lys44	Nζ	Ser64	Oγ	2.85
Arg175	Nη1	Asp168	Oδ2	2.86
Asn176	Nδ2	Ile75	O	2.91
Gln48	O	Lys61	Cε	2.96
Lys44	Nζ	Glu166	Oε1	2.98
Lys61	Nζ	Ile179	OT1	3.12
Gln49	Oε1	Lys61	Nζ	3.15

The distance cutoff of 3.2 Å was used.

Thr53–Arg88 and Glu166–Ile179 in monomer B, has a significant number of hydrophobic residues. Intermolecular interface contacts closer than 3.2 Å are listed in Table 3. The electrostatic and hydrophobic distribution of the hIL-22 surface, together with the position of the principal amino acid residues involved in the formation of the dimer, are given in Figure 3.

Potential Glycosylation Sites

According to the predicted primary structure, human IL-22 has three potential glycosylation sites (Asn-Xaa-Thr/Ser) localized in helix A (Asn54-Arg55-Thr56), loop AB (Asn68-Asn69-Thr70), and helix C (Asn97-Phe98-Thr99). Since the recombinant hIL-22 used in crystallization is not glycosylated, we attempted an analysis of the possible interactions between oligosaccharides and hIL-22 by calculating the accessible area of each residue in all three putative glycosylation sites. The results demonstrate that site 2, localized in loop AB, has a larger accessible area in both the IL-22 dimer and monomer. A solvent-accessible area of approximately 37 Å² was found for the Nδ2 atom of Asn68 and for the Oγ1 atom of Thr70, indicating that there is no steric hindrance to their participation in N-glycosyl and O-glycosyl links, respectively. On the other hand, sites 1 and 3 seem to be able to participate only in N-glycosyl links. The accessible areas of Oγ1-Thr56 and Oγ1-Thr99 are 0 and 6 Å², respectively, both in the monomer and dimer of IL-22, whereas the Nδ2-Asn54 and Nδ2-Asn97 atoms possess, respectively, surface-accessible areas of 24 and 18 Å². This structural analysis is in agreement with biochemical studies suggesting that these three sites are of the N-glycosyl type [4]. The present structure shows that putative glycosylation sites 1 and 2 reside close to the dimer interface, and glycosyl linkages at these positions might hamper dimer formation. It is difficult to conclude whether glycosylation of the protein will interfere with its interactions with receptor chains (see Potential Receptor Binding Sites below) on the basis of the current analysis alone. Further biochemical studies are required to address this question.

Comparison with IL-10 and IFN-γ

The crystallographic structure of hIL-22, as seen in Figure 1B, is a compact dimer with a buried surface area of approximately 2250 Å². Several intermolecular inter-

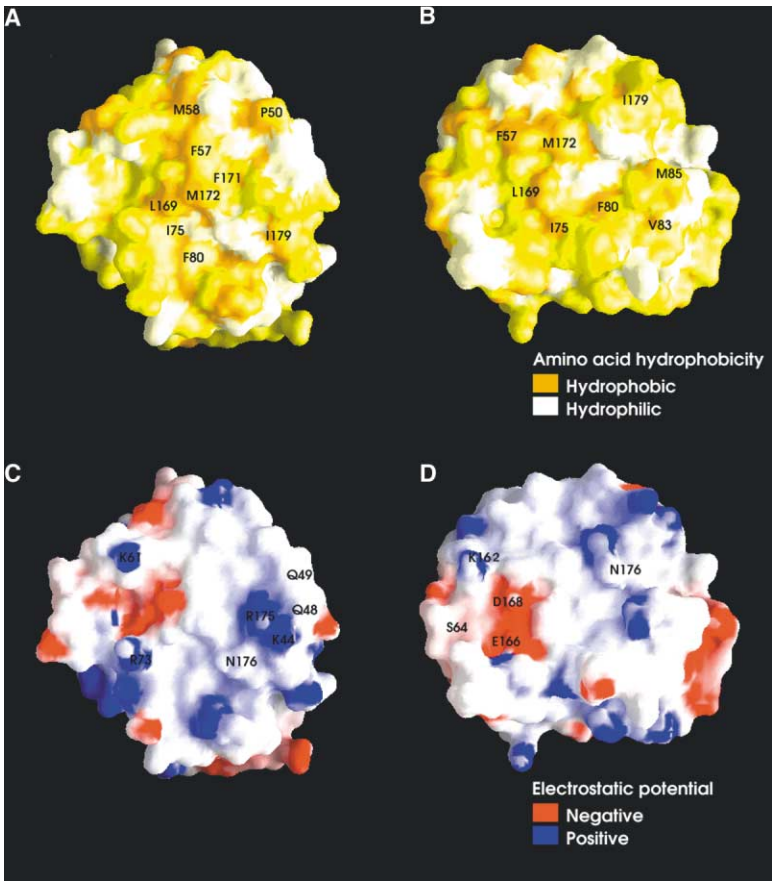

Figure 3. The Contact Surface of the hIL-22 Dimer

The figure is colored according to residue hydrophobicity (A and B) and electrostatic potential (C and D). Interface views of monomer A (A and C) and monomer B (B and D) are shown. In parts (A) and (B), the darker the yellow, the greater the hydrophobicity. In parts (C) and (D), areas of negative, positive, and neutral electrostatic potential are depicted in red, blue, and white, respectively. The figures were prepared with GRASP [32].

actions along the interface surface keep the monomers together. Each monomer, composed of a single domain, is formed by six α helices (A–F) from the same polypeptide chain. In contrast, the crystallographic structures of hIL-10 [11, 12, 13] and hIFN-γ [20, 33] revealed the presence of a homodimer composed of two α-helical domains formed by the intertwining of α helices donated by the first and the second monomer composing a dimer. The first four helices of one chain (A–D) together with helices E′ and F′ from the second chain form the first domain, while helices A′–D′, E, and F form the second domain.

There are, however, significant structural similarities between IL-22, IL-10, and INF-γ (Figure 4). In all these proteins, helices A–D of each monomer form a rigid framework with a highly hydrophobic depression in its middle. This depression is covered in hIL-22 by helices E and F from the same monomer, while, in hIL-10 and hIFN-γ, this is accomplished by helices E′ and F′ (from the second monomer). The basic reason for these differences is in loop DE. There are two cysteine residues, Cys126 and Cys132, in the hIL-10 DE loop that make two distinct disulfide bonds with residues Cys30 and Cys80, respectively. (Here we adopt the residue numbering according to the hIL-10 cDNA sequence). These two disulphide bridges restrict the flexibility of the polipeptide chain and the length of loop DE in such a manner that helices E and F cannot fold onto their respective monomer to occupy position of their counterparts, E′ and F′. This leads to the intertwined dimer formation [11, 12, 13]. A monomeric form of hIL-10 could only be formed if the Cys80-Cys132 disulfide bond were to be reduced or if a small insertion were made after Cys132 [11]. The latter approach has been applied with success to hIL-10, where the insertion of a small polypeptide linker in the loop connecting the swapped secondary structure elements led to the formation of a monomeric protein [34]. Similarly to IL-10, the hIFN-γ intertwined dimer is formed because loop DE is not long enough to allow the folding of helices E and F into the same domain.

In hIL-22 just one disulfide bond (Cys40-Cys132) exists within loop DE. This renders sufficient flexibility and extension of the loop to bring helices E and F into a close interaction with helices A–D and to complete the folding of the monomer. A second disulfide bond (Cys89-Cys178), in the C-terminal of helix F, adds to the rigidity of the final hIL-22 structure.

The best superposition of hIL-22 onto hIL-10 and hIFN-γ, respectively, was obtained using a single domain of the hIL-10 and hIFN-γ dimers and a monomer of hIL-22 (Figures 4A and 4C). The superposition of hIL-10 and hIFN-γ onto hIL-22 yielded an rmsd of 1.9 Å and 2.3 Å for 432 and 300 pairs of main chain atoms, respectively. Helices A–D of the hIL-22 monomer superimpose with helices A–D of one of the monomers of hIL-10 and hIFN-γ. Helices E and F fit nicely into the spatial position occupied by helices E′ and F′ of the second monomer. The 3D superposition of the structures al-

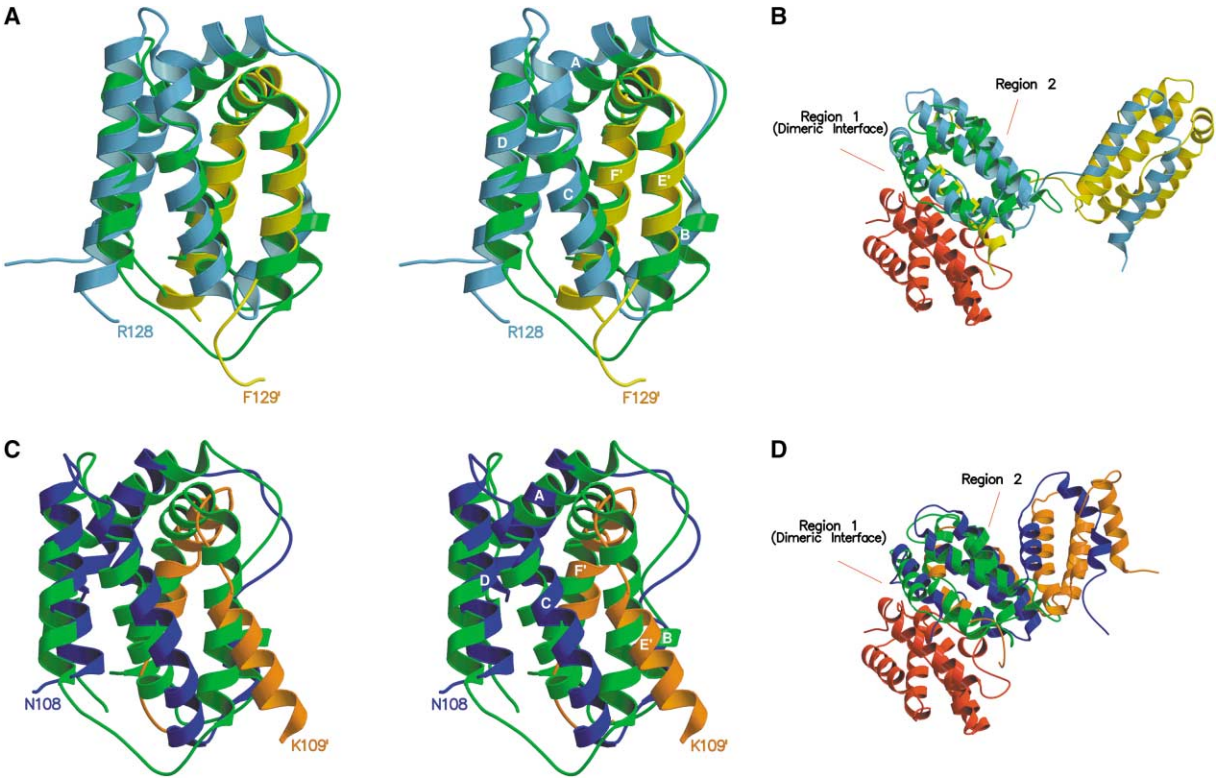

Figure 4. Structural Comparison of hIL-22, hIL-10, and hINF-γ

Ribbon diagram showing the superposition of the hIL-22 monomer (green) onto (A) a single hIL-10 domain (helices A–D, light blue; helices E′–F′, yellow; helices A′–D′, E, and F were omitted) and (C) a single hIFN-γ domain (helices A–D, dark blue; helices E′–F′, orange; helices A′–D′, E, and F were omitted). Superposition of the hIL-22 dimer (individual monomers colored in red and green) onto (B) the hIL-10 dimer (light blue and yellow) and (D) the hIFN-γ dimer (dark blue and orange).

lowed us to perform the structure-based sequence alignment for hIL-22, hIL-10, and hIFN-γ shown in Figure 5. Inspection of the hIL-22 and hIL-10 structure superposition revealed strong similarities in the conformation of the main chain trace of helices E (E′) and F (F′) and, to a lesser extent, several parts of loop AB, helix C, and helix D. As can be seen in the sequence alignment, all these regions have high sequence similarity. Some significant differences in the regions of the N-terminal coil, helix A, helix B, loop BC, loop CD, and, clearly, loop DE were also observed.

Reasonable superposition of hIL-10 or hIFN-γ dimers onto the hIL-22 dimer has proven to be impossible. The dimer formation in each case is so different that only one monomer of hIL-22 could be superimposed with one domain from hIL-10 or hIFN-γ, while the second domain of these structures occupies a completely different spatial position (Figures 4B and 4D). In hIL-10 and hIFN-γ the intertwining of α helices is essential for the formation and integrity of the molecules, which assume the form of V-shaped dimers, while dimer formation is not required for folding in hIL-22. It must be stressed that the buried surface on the hIL-22 interface coincides with the part of the external surface of the hIL-10 and hIFN-γ V-shaped dimer surfaces (Figures 4B and 4D).

Potential Receptor Binding Sites

Two receptor chains have been identified for IL-22, namely, CRF2-9 and CRF2-4. The second receptor chain is common to IL-22 and IL-10 and is necessary for signaling, whereas the first one is specific for IL-22 [3, 4] and shows some primary sequence homology with another receptor chain of IL-10 (the IL-10R1). The binding affinity of IL-22 and IL-10 to CRF2-4 seems different. CRF2-4 alone is sufficient to bind IL-22, while the presence of a second receptor chain is required for efficient IL-10 binding. Moreover, CRF2-9 and CRF2-4 present significant sequence homology to the INF-γ receptor, INF-γRα. The three-dimensional structure of hINF-γRα has been solved as a complex with its ligand [20]. The structure of hIL-22 was superimposed onto the structure of hINF-γ/hINF-γRα complex in order to identify the residues putatively involved in the hIL-22/receptor interactions. A similar structural comparison using the hGH/hGHBP complex had been used previously in the putative receptor binding sites analysis of IL-10 [11].

The superposition of hIL-22 onto the hINF-γ/hINF-γRα complex indicates that one possible receptor binding site is localized in the region formed by helix A, loop AB, and helix F of hIL-22 (region 1, R1; see Figures 4D, 6A, and 6B). Among the 17 residues involved in hINF-γ/hINF-γRα interactions (closer than 3.4 Å), only 2 residues do not have their hIL-22 structural counterparts localized in R1. Nine of the 17 residues localized in R1 are not sufficiently close to their hINF-γ counterparts, which may explain the inability of hIL-22 to bind to hINF-γRα. The major differences between hINF-γ and hIL-22 within R1 are observed in loop AB. Distances of more than

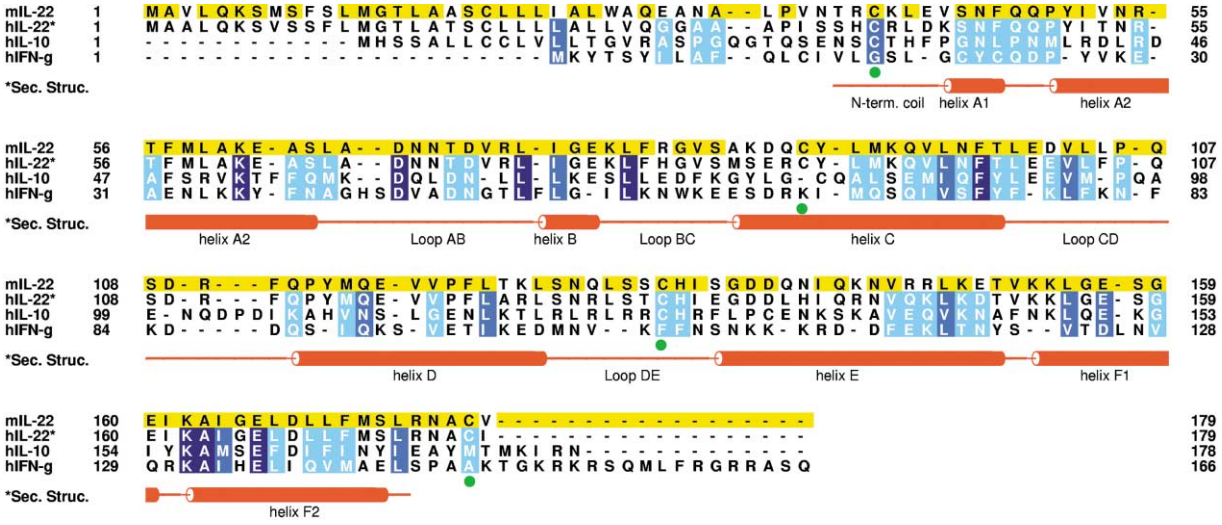

Figure 5. Primary Structure Alignment of Murine IL-22, Human IL-22, Human IL-10, and Human IFN-γ

Whenever possible the three-dimensional information was used to improve the alignment. Disulfide bonds in hIL-22 are marked with green circles. The amino acid similarity between hIL-22, hIL-10, and hIFN-γ, as calculated by the program ALSCRIPT [35], is shown in three different shades of blue. The darker color corresponds to higher sequence similarity. Residues conserved in mIL-22 and hIL-22, yellow; human IL-22 secondary structure elements, red. The figure was drawn using the program ALSCRIPT.

7 Å are found between their main chains. However, six relatively conserved residues (Lys61, Thr70, Asp71, Lys162, Glu166, and Leu169) occupy almost the same spatial position as six hINF-γ residues (Lys35, Asp47, Asn48, Lys131, Glu135, and Gln138; cDNA numbering), as can be seen in Figure 6A.

A comparison with the hIL-10 putative receptor binding site [11] shows that the same region 1 (helix A, loop AB, and helix F′ in the case of hIL-10) should be involved in receptor interactions. Amino acid residues Gln60, Asp62, Asn63, Lys156, Glu160, Asp162, Asn166, and Glu169 of the hIL-10 binding site have their hIL-22 counterparts in residues Asn68, Thr70, Asp71, Lys162, Glu166, Asp168, Met172, and Arg175. Among these eight residues, four of them (Thr70, Asp71, Lys162, and Glu166) were also found in the hIL-22:INF-γ/INF-γRα structure comparison.

After the current structure was determined and its structural comparison with the hINF-γ/hINF-γRα and hGH/hGHBP complexes had been performed, the crystallographic structure of the IL-10/IL-10R1 became available [21]. The structure of this complex confirms that the prime binding site of the IL-10 with its high-affinity receptor (site 1a) includes residues Gln56, Gln60, Asp62, Asn63, Lys156, Ser159, Glu160, and Asp162, corresponding to amino acid residues Ser64, Asn68, Thr70, Asp71, Lys162, Gly165, Glu166, and Asp168 in hIL-22. Of these, three amino acid residues, Ser64, Glu166, and Asp168, are involved in intermolecular contacts at the homodimer interface of the current IL-22 structure (Table 3). Besides this, Asp168 and Glu166 of monomer B form salt bridges with Arg175 of the neighboring monomer, A. Arg175, therefore, occupies a position equivalent to that of Arg96 of the IL-10R1 receptor in the IL-10/IL-10R1 complex. Arg96 is one of the most important residues involved in the IL-10/Il-10R1 complex formation, as it forms an extensive hydrogen bond network with Asp162, Gln56, and the main chain carbonyl oxygen of Ser159 from IL-10 [21]. Remarkably, sequence alignment shows that the CRF2-9 receptor chain contains an arginine residue homologous to Arg96 of IL-10R1. One may infer, therefore, that Arg 175 of IL-22 monomer A binds to residues Glu166 and Asp168 of IL-22 monomer B in a way that resembles CRF2-9 binding to this cytokine (Figure 6C).

Amino acid residues Pro38, Arg42, Arg45, and Glu169 form the 1b subsite in the IL-10/IL-10R1 structure. These residues are equivalent to Gln48, Ile52, Arg55, and Arg175 of the IL-22 molecule. Gln48 and Arg175 of IL-22 monomer A again form part of the dimer interface interacting with the residues Lys61, Glu166, and Glu168 of monomer B (Table 3). This means that a large part of the IL-22 homodimer interface is formed by interactions of the amino acid residues potentially involved in receptor binding.

The structural comparison of hIL-22 with the hINF-γ/hINF-γRα and IL-10/IL-10R1 complexes leaves little doubt that region 1 is a putative receptor binding site. The three-dimensional and amino acid sequence similarities observed between hIL-22, hIL-10, and INF-γ, respectively, in region 1, especially between helices F and F′, indicate that this region might serve as the high-affinity receptor binding site. Further support for this hypothesis comes from the similarities in amino acid sequence of IL-10R1, CRF2-9, and INF-γRα, particularly in the loop regions involved in the interactions with the respective cytokines [21]. However, the differences observed in loop AB, including the presence of a potential glycosylation site in hIL-22 and, also, the lack of sufficient biochemical data, do not allow us to definitively infer which receptor chain binds region 1 of hIL-22. In fact, considering the hypothesis that the glycosylation site in the hIL-22 AB loop may affect receptor recognition and also that IL-10R1 and INF-γRα have low, but

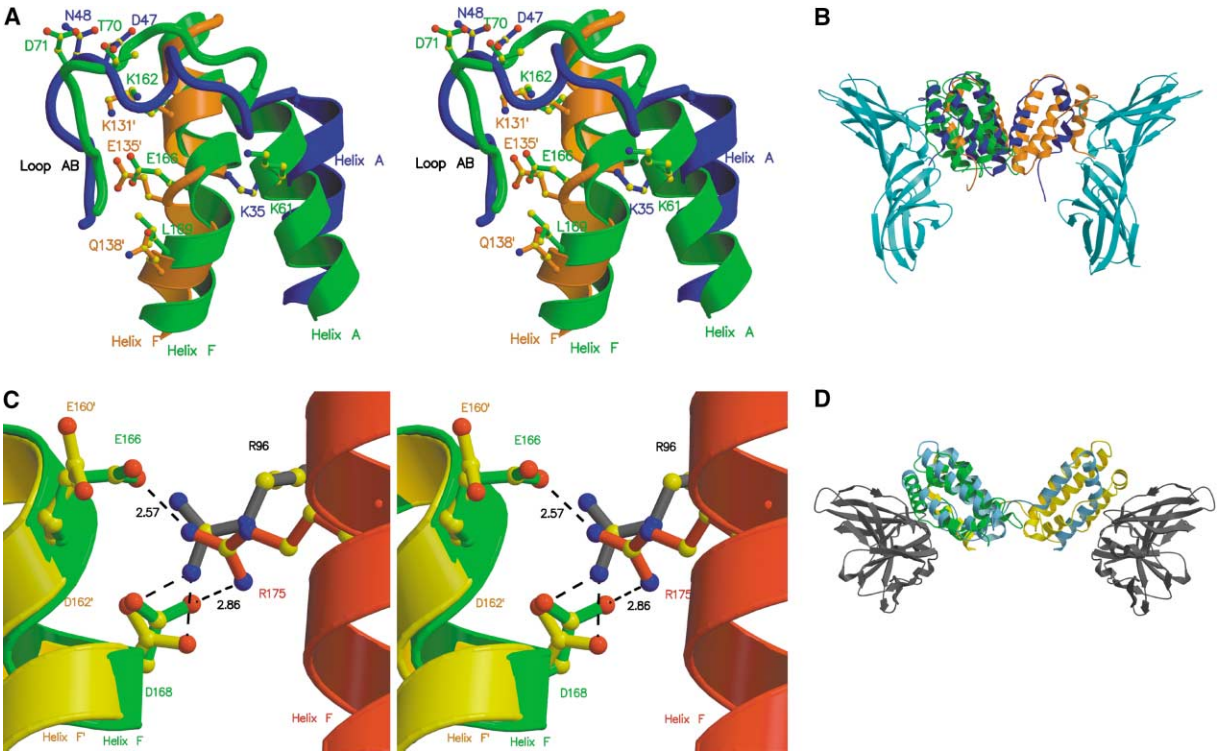

Figure 6. Molecular Details of the Putative Receptor Binding Site (R1) of IL-22

(A) Superposition of the hIFN-γ/hIFN-γRα complex. hIFN-γ, dark blue and orange; hIL-22 monomer, green. Amino acid residues forming the putative receptor binding site of IL-22 and the binding site of hIFN-γ to the hIFN-γRα receptor are represented by ball and stick diagrams, colored according to the molecule coloring scheme and labeled.

(B) Ribbon diagram of hIFN-γ bound to the hIFN-γRα receptor. hIFN-γ, dark blue and orange; hIFN-γRα, cyan. The hIL-22 monomer (green) is superimposed with one of the hIFN-γ domains.

(C) Superposition of hIL-22 onto hIL-10. Only residues Glu160 and Asp162 of the hIL-10 receptor binding site 1a and residue Arg96 of hIL-10R1 are shown superimposed onto the hIL-22 putative binding site residues Glu166 and Asp168 of monomer B and amino acid residue Arg175 of monomer A. Note that the amino acid residue Arg175 at the hIL-22 homodimer interface in the hIL-22 dimer structure mimics hIL-10R1 Arg96 interactions with the correspondent residues of the hIL-10 1a binding site in the hIL-10/Il-10R1 complex [21]. hIL-10, gold; hIL-22 monomer A, red; hIL-22 monomer B, green; IL-10R1 residue Arg96, gray. Numbers in black show distances in Å.

(D) A ribbon diagram of hIL-10 bound to the hIL-10R1 receptor. hIL-10, light blue and gold; hIL-10R1, gray; hIL-22 monomer, superimposed with one of the hIL-10 domains, green.

detectable, similarity to CRF2-4, one may suggest that R1 could also be the recognition/binding site for CRF2-4. This hypothesis also finds support in the model for the IL-10/IL-10R1/CRF2-4 complex, where both receptors share the same binding site [21].

In the present crystallographic model, region 1 of each monomer is hidden at the dimer interface. Moreover, a number of potential receptor binding residues are directly involved in the dimer formation (see Table 3). Therefore, an hIL-22 receptor chain could only bind a monomer of hIL-22, which would require dissociation of the dimer observed in the present crystallographic structure. In contrast, the hIL-10 and hIFN-γ dimers do not require dissociation in order to interact with their receptor, since their high affinity receptor binding sites are located on the external part of the V-shaped dimer surface.

To further assess the oligomerization state of hIL-22 in solution, gel filtration and dynamic light-scattering (DLS) studies were undertaken. The state of oligomerization of the protein was found to be concentration dependent. The initial protein concentration applied to the gel filtration column was 1 mg/ml, and the eluted recombinant IL-22 sample had an apparent molecular weight of 15 kDa and was fully active.

DLS measurements performed at a protein concentration of 5 mg/ml resulted in an apparent Stokes radius of 2.08 ± 0.06 nm, which corresponds to a standard molecular weight of approximately 19 kDa. This demonstrates that hIL-22 was present in solution predominantly in a monomeric form, in line with the results of the gel filtration studies. An excellent correlation with the Stokes radius of 2.11 nm calculated using the HYDROPRO program [36] on the basis of the crystal structure of the monomer determined in the present work further confirms this conclusion. Therefore, both gel filtration and DLS studies demonstrate that hIL-22 is a monomer at physiologically relevant concentrations (≤5 mg/ml).

The DLS measurements performed on the protein sample concentrated to 10 mg/ml resulted in a Stokes radius of 2.74 ± 0.06 nm and an apparent molecular weight of 35.5 kDa, suggesting that a dimer is the predominant oligomeric form under these conditions. The

apparent Stokes radius of 2.58 nm computed by HYDROPRO from the crystallographic model of the dimer occupying the asymmetric unit is in agreement with the experimental results. This indicates not only that, under conditions of crystallization, hIL-22 predominantly forms dimers in solution, but also that the calculated hydrodynamic parameters of the dimers observed in the crystal are close to the experimentally determined hydrodynamic parameters of the dimers observed in solution.

Assuming that the CRF2-4 and CRF2-9 receptor chains have separate binding sites, there should be at least two distinct sites for receptor binding to the IL-22 molecule. A second possible binding site in hIL-22 could not be easily identified from inspection of the interactions between hINF-γ and hINF-$\gamma R\alpha$ or hIL-10 and hIL-10R1. Nevertheless, the C-terminal parts of helices C and E of each hIL-22 monomer could be another potential binding site (region 2, R2) for the common receptor chain (CRF2-4). A sequence comparison between hIL-22 and several IL-10s shows that several amino acids are conserved within R2 (sequences FTLEEVL and KLGE in hIL-22 helices C and E, respectively). These regions (R2) are localized at the surface of the IL-22 opposite from R1. Localization of each putative binding region (R1 and R2) on the opposite sides of the hIL-22 molecule would allow for interaction with two receptor chains simultaneously. The hIL-10 R2 counterparts are localized at the inner part of the V-shaped dimer surface. The angle between each hIL-10 domain in the V-shaped dimer could be large enough to allow for the interaction of two CRF2-4 receptor chains with the two putative binding sites at R2 (Figure 4B).

Biological Implications

Cytokines are proteins that exert their action by binding to specific cell surface receptors, leading to the activation of cytokine-specific signal transduction pathways. These proteins play several important biological roles, including multiple and generally immunosuppressive activities, immunomodulatory and antiviral effects, and stimulation of T cell growth, among others [37]. IL-22 is a new cytokine expressed in T cells upon activation by IL-9 and in mast cell, thymus, and brain upon activation by concanavalin A (ConA), indicating that this factor might exhibit pleiotropic activities, within and outside of the immune system [1]. Two different receptor chains, CRF2-9 and CRF2-4, have been identified as components of the IL-22 signaling complex [3, 4]. A role for this protein in inflammatory processes has been suggested after observing that IL-22 induces STAT activation and upregulates acute phase reactant production by liver cells [2].

Here we report the first crystallographic structure of this new cytokine, human IL-22. Possible receptor binding sites were identified via comparison with the related complex structures of hIFN-γ/hIFN-$\gamma R\alpha$ and hIL-10/hIL-10R1.

hIL-22 is a compact molecule of a single domain composed of six α helices. A dimer of human IL-22 was found in the asymmetric unit of the crystal. Unlike IL-10 and IFN-γ, which are V-shaped homodimers of two interpenetrating polypeptide chains, the hIL-22 dimer is comprised of two independent monomers held together by intermolecular interactions. No intertwining of α helices was observed in the crystallographic structure of hIL-22.

The superposition of hIL-22 onto the hIFN-γ/hIFN-$\gamma R\alpha$ and hIL-10/hIL-10R1 complexes allowed us to identify a possible hIL-22 receptor binding site (region 1, R1). This site is comprised of helix A, loop AB, and helix F, similarly to the first binding site reported for hIL-10 [11, 21]. The overall similarity of hIL-22 to hIL-10, especially in the region of this putative receptor binding site and, also, in their respective high-affinity receptors (CRF2-9 and IL-10R1), indicates that this site could represent the binding site for CRF2-9. However, the lack of biological studies does not allow us to unambiguously conclude whether this is a binding site for the CRF2-9 or CRF2-4 receptor chains or the common binding site for both of these receptors [21]. Remarkably, the receptor binding site in R1 is occluded in the hIL-22 structure as a consequence of dimer formation. This leads us to propose that the active species of hIL-22 is a monomer. This is in a perfect agreement with the results of gel filtration and DLS studies demonstrating that hIL-22 is a monomer at physiologically relevant concentrations. Several other cytokines have already been shown to dimerize at high concentrations while being biologically active as monomers (see, for example, [38] and [39] and the references therein). An observation that an engineered human IL-10 monomer is biologically active in cellular proliferation assays further corroborates this hypothesis [34].

Another putative binding region (region 2, R2) for CRF2-4 (or IL-10R2) was identified on hIL-22 by surface-mapped sequence comparison with hIL-10. R2 is localized on the opposite side from the first binding site (region 1, R1), leaving enough room for binding for a second receptor. Primary structure comparison of several IL-10s and IL-22s from different organisms indicates that the residues forming the second putative binding site are highly conserved.

The structure of hIL-22 presented here brings us closer to an understanding of its interactions with its receptor chains and the mechanism of signal transduction exerted by this molecule. Moreover, this structural information may help in the solution of the structure of the IL-22:receptor complex and also offers the possibility of structure-based site-directed-mutagenesis mapping of the receptor binding sites.

Experimental Procedures

Protein Expression and Purification

Recombinant human IL-22 was produced in *E. coli* as follows. The IL-22 sequence (corresponding to amino acids Q29–I179) was amplified by PCR from a cDNA clone using primers hTIFa (5′-GGCCCTC TTGGTACATATGCAGGGAGGAGCAGCTGCG-3′) and hTIFb (5′-CAG CTTTGCTCTGGGGATCCTTATCAAATGCAGGCATTTCTCAG-3′). The PCR product was digested with NdeI and BamHI and cloned into the pET3A plasmid (Stratagene, La Jolla, CA). *E. coli* strain BL21-codon plus-(DE3)-RIL (Stratagene) was used as the expression host. The cells were grown in LB medium supplemented with 100 μg/ml ampicillin and 34 μg/ml chloramphenicol. Expression of IL-22 was induced with 1 mM IPTG at a cell density (600 nm) of $\sim$1. Cells were collected by centrifugation 4 hr after induction. The cell pellet was

disrupted with a high-pressure cell homogenizer, and the IL-22 inclusion bodies were collected by centrifugation. Inclusion bodies were washed extensively, first with 50 mM Tris-HCl, 100 mM NaCl, 1 mM EDTA, 1 mM DTT, and 0.5% (w/v) DOC (pH 8) and finally with the same buffer without detergent. Inclusion bodies were solubilized overnight at 4°C in 8 M urea, 50 mM MES, 10 mM EDTA, and 0.1 mM DTT (pH 5.5). The solution was centrifuged for 1 hr at 100,000 × g, and the supernatant was stored at −80°C until use. The purity of the IL-22 was estimated at ~80% based on SDS-PAGE and Coomassie blue staining analysis. The concentration of protein was estimated by UV absorbance in urea solution using a calculated $\epsilon_{280} = 3840$. The IL-22 protein was refolded by direct dilution of the solubilized inclusion bodies in the following folding mixture: 100 μg/ml IL-22, 100 mM Tris-HCl, 2 mM EDTA, 0.5 M L-Arginine, 1 mM reduced glutathion, and 0.1 mM oxidized glutathion (pH 8). The solution was incubated for 72 hr at 4°C. The folding mixture was then concentrated by ultrafiltration in an AMICON chamber with a YM3 membrane before purification on a Superdex75 (Amersham Pharmacia Biotech) gel filtration column. The protein was eluted with 25 mM MES and 150 mM NaCl (pH 5.4). The protein bioactivity was assessed following procedures previously described [40]. The recombinant protein was found to be fully active. Human IL-22 peak fractions were concentrated to 5 mg/ml with a YM3 AMICON membrane and desalted using a Hiprep 26/10 column (Amersham-Pharmacia) with elution buffer containing 10 mM MES (pH 5.4). Human IL-22 was concentrated again to 5 mg/ml and lyophilized in 1 mg fractions.

Protein Crystallization

Preliminary screening of the crystallization conditions was performed using a sparse-matrix screen at 291 K (Crystal Screen I and II; Hampton Research). Small crystals were found in the conditions 18, 26, and 29 of the Crystal Screen I kit. Several attempts to enhance crystal quality were performed, including pH and precipitant concentration refinement, detergent addition, and macroseeding. Well-diffracting crystals were obtained in hanging drops equilibrated against a reservoir solution consisting of 0.9 M sodium tartrate, TRITON X-100 detergent, and 0.1 M HEPES (pH 7.5). The crystallization drops contained equal volumes (1 μl) of reservoir and purified hIL-22 (10 mg/ml in 20 mM MES buffer at pH 5.4) solutions. The protein crystallized in the space group $P2_12_12_1$, with unit cell dimensions a = 55.43, b = 61.61, and c = 73.43 Å.

Data Collection

Crystals were soaked in different cryosoaking solutions, mounted in rayon loops, and, finally, flash-cooled to 80 K in a cold nitrogen stream. Data collection was performed at the Protein Crystallography beamline (LNLS, Campinas, Brazil [22, 23]) and at the X4A beamline (NSLS, Upton, New York) using a MAR345 image plate and a Quantum-4 CCD detector, respectively. Three diffraction datasets were collected to a maximum resolution beyond 1.95 Å. Diffraction images were processed and scaled with the programs DENZO and SCALEPACK [41].

Heavy-Atom Derivatives and Phasing

The structure was solved by SIRAS. An iodine derivative was obtained by soaking the crystal for 180 s in 2 μl of cryoprotectant solution containing 0.125 M sodium iodide following a novel derivatization procedure named "quick cryosoaking" [24, 25]. One weak mercury derivative was also obtained using traditional methods of derivatization. However, this derivative did not provide independent phase information and was used as a quasi-native dataset. The heavy-atom positions of the iodine derivative were determined by direct methods with the programs DREAR [42] and SnB 2.1 [43]. The bimodal distribution of the R_{min} histogram was used to identify the correct solution [44, 45]. The heavy-atom substructure obtained directly from SnB was initially refined with the CNS package using anomalous and isomorphous difference Fourier maps. Refined coordinates were then input into SHARP [46] for phase calculation, resulting in an overall figure of merit of 0.45 for all reflections in the range of 21.7–2.40 Å. Density modification with solvent flattening was performed using the program SOLOMON [47].

Model Building and Refinement

A solvent-flattened electron density map and structure factor amplitudes from the iodine derivative were used by the ARP/wARP program [26] for an automatic build of a hybrid model of hIL-22. Due to the high resolution and completeness of the I-hIL-22 data set, an initial model was obtained without manual intervention after six ARP/wARP jobs and more than 4000 REFMAC [48] cycles. In the last cycle, after almost 72 hr of uninterrupted CPU time on a Pentium III 500 MHz, 81.6% of the total amino acid residues were correctly traced.

The initial model contained 231 amino acid residues (in nine distinct chains) and 809 water molecules. To avoid modeling of a large number of partially occupied iodine ions that were present at the concentration of 125 mM in the cryosolution of this derivative, subsequent refinement was performed against the Nat-hIL-22 data set. Construction of disordered loops and filling of main chain gaps were performed manually using the program O [49], and the CNS refinement against the Nat-hIL-22 and Hg-hIL-22 (quasi-native) data sets was performed when judged necessary. This allowed for a complete trace of the main chain atoms through disordered regions. Independent refinement of the model against I-hIL-22 data resulted in higher R factor and R_{free} values, due to a large number of halides with partial occupancies bound to the protein found in the electron density maps. After several iterations of energy minimization, B factor refinement, and bulk-solvent and anisotropic corrections, the final R factor and R_{free} against the Nat-hIL-22 data set were 0.188 and 0.220, respectively. The final model includes 283 residues divided into two chains and 189 water molecules.

Protein Oligomerization State

The protein oligomerization state has been assessed by gel filtration and dynamic light-scattering (DLS) studies. Gel filtration experiments were conducted in the conditions described in Protein Expression and Purification. DLS measurements have been performed with a DynaPro MS200 instrument (Protein Solutions) at 20°C using a 12 μl cuvette. The protein samples were concentrated to 5 mg/ml and 10 mg/ml in 0.1 M HEPES buffer at pH 7.5 prior to measurements.

Acknowledgments

The authors are grateful to J.R. Brandão Neto and Zbigniew Dauter for help with data collection, Katucha W. Lucchesi and Miroslawa Dauter for help with crystallization of the proteins, Dr. Nilson I.T. Zanchin and Profs. Munro Neville, Ricardo R. Brentani, and Rogério Meneghini for comments and suggestions, and Prof. Richard C. Garratt for style and grammar corrections. Financial help from CNPq and FAPESP (via grants 99/03387-4 and 98/06218-6) is acknowledged.

Received: November 16, 2001
Revised: April 30, 2002
Accepted: May 14, 2002

References

1. Dumoutier, L., Louahed, J., and Renauld, J.C. (2000). Cloning and characterization of IL-10-related T cell-derived inducible factor (IL-TIF), a novel cytokine structurally related to IL-10 and inducible by IL-9. J. Immunol. *164*, 1814–1819.
2. Dumoutier, L., Van Roost, E., Colau, D., and Renauld, J.C. (2000). Human interleukin-10-related T cell-derived inducible factor: molecular cloning and functional characterization as an hepatocyte-stimulating factor. Proc. Natl. Acad. Sci. USA *97*, 10144–10149.
3. Xie, M.H., Aggarwal, S., Ho, W.H., Foster, J., Zhang, Z., Stinson, J., Wood, W.I., Goddard, A.D., and Gurney, A.L. (2000). Interleukin (IL)-22, a novel human cytokine that signals through the interferon receptor-related proteins CRF2–4 and IL-22R. J. Biol. Chem. *275*, 31335–31339.
4. Kotenko, S.V., Izotova, L.S., Mirochnitchenko, O.V., Esterova, E., Dickensheets, H., Donnelly, R.P., and Pestka, S. (2001). Iden-

tification of the functional interleukin-22 (IL-22) receptor complex. J. Biol. Chem. *276*, 2725–2732.
5. Kotenko, S.V., and Pestka, S. (2000). Jak-stat signal transduction pathway through the eyes of cytokine class II receptor complexes. Oncogene *19*, 2557–2565.
6. Gallagher, G., Dickensheets, H., Eskdale, J., Izotova, L.S., Mirochnitchenko, O.V., Peat, J.D., Vazquez, N., Pestka, S., Donnelly, R.P., and Kotenko, S.V. (2000). Cloning, expression and initial characterization of interleukin-19 (IL-19), a novel homologue of human interleukin-10 (IL-10). Genes Immun. *1*, 442–450.
7. Blumberg, H., Conklin, D., Xu, W.F., Grossmann, A., Brender, T., Carollo, S., Eagan, M., Foster, D., Haldeman, B.A., Hammond, A., et al. (2001). Interleukin-20: discovery, receptor identification and role in epidermal function. Cell *104*, 9–19.
8. Jiang, H., Lin, J.J., Su, Z.Z., Goldstein, N.I., and Fisher, P.B. (1995). Subtraction hybridization identifies a novel melanoma differentiation associated gene, mda-7, modulated during human progression. Oncogene *11*, 2477–2486.
9. Moore, K.W., de Waal Malefyt, R., Coffman, R.L., and O'Garra, A. (2001). Interleukin-10 and the interleukin-10 receptor. Annu. Rev. Immun. *19*, 683–765.
10. Fickenscher, H., Hor, S., Kupers, H., Knappe, A., Wittmann, S., and Sticht, H. (2002). The interleukin-10 family of cytokines. Trends Immunol. *23*, 89–96.
11. Zdanov, A., Schalk-Hihi, C., Gustchina, A., Tsang, M., Weatherbee, J., and Wlodawer, A. (1995). Interleukin-10: crystal structure reveals the functional dimer with an unexpected topological similarity to interferon gamma. Structure *3*, 591–601.
12. Zdanov, A., Schalk-Hihi, C., and Wlodawer, A. (1996). Crystal structure of human interleukin-10 at 1.6 Å resolution and a model of a complex with its soluble receptor. Protein Sci. *5*, 1955–1962.
13. Walter, M.R., and Nagabhushan, T.L. (1995). Crystal-structure of interleukin-10 reveals an interferon gamma-like fold. Biochemistry *34*, 12118–12125.
14. Zdanov, A., Schalk-Hihi, C., Menon, S., Moore, K.W., and Wlodawer, A. (1996). Crystal structure of Epstein-Barr virus protein BCRF1, a homolog of cellular interleukin-10. J. Mol. Biol. *268*, 460–467.
15. Temann, U.A., Geba, G.P., Rankin, J.A., and Flavell, R.A. (1998). Expression of interleukin-9 in the lungs of transgenic mice causes airway inflammation, mast cell hyperplasia, and bronchial hyperresponsiveness. J. Exp. Med. *188*, 1307–1320.
16. McLane, M.P., Haczku, A., van de Rijn, M., Weiss, C., Ferrante, V., MacDonald, D., Renauld, J.C., Nicolaides, N.C., Holroyd, K.J., and Levitt, R.C. (1998). Interleukin-9 promotes allergen-induced eosinophilic inflammation and airway hyperresponsiveness in transgenic mice. Am. J. Respir. Cell Mol. Biol. *19*, 713–720.
17. Dumoutier, L., Van Roost, E., Ameye, G., Michaux, L., and Renauld, J.C. (2000). IL-TIF/IL-22: genomic organization and mapping of the human and mouse genes. Genes Immun. *1*, 488–494.
18. Renauld, J.C. (2001). New insights into the role of cytokines in asthma. J. Clin. Pathol. *54*, 577–589.
19. Kotenko, S.V., Krause, C.D., Izotova, L.S., Pollack, B.P., Wu, W., and Pestka, S. (1997). Identification and functional characterization of a second chain of the interleukin-10 receptor complex. EMBO J. *16*, 5894–5903.
20. Thiel, D.J., le Du, M.H., Walter, R.L., D'Arcy, A., Chene, C., Fountoulakis, M., Garotta, G., Winkler, F.K., and Ealick, S.E. (2000). Observation of an unexpected third receptor molecule in the crystal structure of human interferon-gamma receptor complex. Structure *8*, 927–936.
21. Josephson, K., Logsdon, N.J., and Walter, M.R. (2001). Crystal structure of the IL10-IL-10R1 complex reveals a shared receptor binding site. Immunity *14*, 35–46.
22. Polikarpov, I., Perles, L.A., de Oliveira, R.T., Oliva, G., Castellano, E.E., Garratt, R.C., and Craievich, A. (1997). Set-up and experimental parameters of the protein crystallography beamline at the Brazilian National Synchrotron Laboratory. J. Synchrotron Radiat. *5*, 72–76.
23. Polikarpov, I., Oliva, G., Castellano, E.E., Garratt, R.C., Arruda, P., Leite, A., and Craievich, A. (1997). The protein crystallography beamline at LNLS, the Brazilian National Synchrotron Light Source. Nucl. Instrum. Methods Phys. Res. A *405*, 159–164.
24. Dauter, Z., Dauter, M., and Rajashankar, K.R. (2000). Novel approach to phasing proteins: derivatization by short cryo-soaking with halides. Acta Crystallogr. D Biol. Crystallogr. *56*, 232–237.
25. Nagem, R.A.P., Dauter, Z., and Polikarpov, I. (2001). Protein crystal structure solution by fast incorporation of negatively and positively charged anomalous scatterers. Acta Crystallogr. D Biol. Crystallogr. *57*, 996–1002.
26. Perrakis, A., Morris, R., and Lamzin, V.S. (1999). Automated protein model building combined with iterative structure refinement. Nat. Struct. Biol. *6*, 458–463.
27. Brunger, A.T., Adams, P.D., Clore, G.M., DeLano, W.L., Gros, P., Grosse-Kunstleve, R.W., Jiang, J.S., Kuszewski, J., Nilges, M., Pannu, N.S., et al. (1998). Crystallography and NMR system: a new software suite for macromolecular structure determination. Acta Crystallogr. D Biol. Crystallogr. *54*, 905–921.
28. Laskowski, R.A., MacArthur, M.W., Moss, D.S., and Thornton, J.M. (1993). PROCHECK: a program to check the stereochemical quality of protein structures. J. Appl. Crystallogr. *26*, 283–291.
29. Kraulis, P.J. (1991). Molscript—a program to produce both detailed and schematic plots of protein structures. J. Appl. Crystallogr. *24*, 946–950.
30. Esnouf, R.M. (1997). An extensively modified version of Molscript that includes greatly enhanced coloring capabilities. J. Mol. Graph. *15*, 133–138.
31. Merritt, E.A., and Bacon, D.J. (1997). Raster3D: photorealistic molecular graphics. Methods Enzymol. *277*, 505–524.
32. Nicholls, A., Sharp, K.A., and Honing, B. (1991). Protein folding and association—insights from the interfacial and thermodynamic properties of hydrocarbons. Proteins: Struct. Funct. Genet. *11*, 281–296.
33. Ealick, S.E., Cook, W.J., Vijay-Kumar, S., Carson, M., Nagabhushan, T.L., Trotta, P.P., and Bugg, C.E. (1991). Three-dimensional structure of recombinant human interferon-gamma. Science *252*, 698–702.
34. Josephson, K., DiGiacomo, R., Indelicato, S.R., Iyo, A.H., Nagabhushan, T.L., Parker, M.H., Walter, M.R., and Ayo, A.H. (2000). Design and analysis of an engineered human interleukin-10 monomer. J. Biol. Chem. *275*, 13552–13557.
35. Barton, G. (1993). ALSCRIPT: a tool to format multiple sequence alignments. Protein Eng. *6*, 37–40.
36. Garcia de La Torre, J., Huertas, M.L., and Carrasco, B. (2000). Calculation of hydrodynamic properties of proteins from their atomic level structures. Biophys. J. *78*, 719–730.
37. Trèze, J. (1999). The Cytokine Network and Immune Functions (Oxford: Oxford University Press).
38. Goger, B., Halden, Y., Rek, A., Mosl, R., Pye, D., Gallagher, J., and Kungl, A.J. (2002). Different activities of glycosaminoglycan oligosaccharides for monomeric and dimeric interleukin-8: a model for chemokine regulation at inflammatory sites. Biochemistry *41*, 1640–1646.
39. Laurence, J.S., Blanpain, C., Burgner, J.W., Parmentier, M. and LiWang, P.J. (2000). CC chemokine MIP-1β can function as a monomer and depends on Phe13 for receptor binding. Biochemistry *39*, 3401–3409.
40. Dumoutier, L., Lejeune, D., Colau, D., and Renauld, J.-C. (2001). Cloning and characterization of Interleukin-22 binding protein (IL-22BP), a natural antagonist of IL-TIF/IL-22. J. Immunol. *166*, 7090–7095.
41. Otwinowski, Z., and Minor, W. (1997). Processing of X-ray diffraction data collected in oscillation mode. Methods Enzymol. *276*, 307–326.
42. Blessing, R.H., and Smith, G.D. (1999). Difference structure-factor normalization for heavy-atom or anomalous-scattering substructure determinations. J. Appl. Crystallogr. *32*, 664–670.
43. Weeks, C.M., and Miller, R. (1999). The design and implementation of SnB version 2.0. J. Appl. Crystallogr. *32*, 120–124.
44. Debaerdemaeker, T., and Woolfson, M.M. (1983). On the application of phase-relationships to complex structures. Techniques for random phase refinement. Acta Crystallogr. A *39*, 193–196.
45. De Titta, G.T., Weeks, C.M., Thuman, P., Miller, R., and Hauptman, H.A. (1994). Structure solution by minimal-function phase

refinement and Fourier filtering. Theoretical basis. Acta Crystallogr. A *50*, 203–210.
46. de La Fortelle, E., and Bricogne, G. (1997). Maximum-likelihood heavy-atom parameter refinement for multiple isomorphous replacement and multiwavelength anomalous diffraction methods. Methods Enzymol. *276*, 472–494.
47. Abrahams, J.P., and Leslie, A.G.W. (1996). Methods used in the structure determination of bovine mitochondrial F-1 ATPase. Acta Crystallogr. D Biol. Crystallogr. *52*, 30–42.
48. Murshudov, G.N., Vagin, A.A., and Dodson, E.J. (1997). Refinement of macromolecular structures by the maximum-likelihood method. Acta Crystallogr. D Biol. Crystallogr. *53*, 240–255.
49. Jones, T.A., Zou, J.Y., Cowan, S.W., and Kjeldgaard, M. (1991). Improved methods for building protein models in electron-density maps and the location of errors in these models. Acta Crystallogr. A *47*, 110–119.

Accession numbers

The atomic coordinates and the structure factors are deposited with the Protein Data Bank under accession code 1M4R (RCSB ID code RCSB016596).